A Journal of the Gesellschaft Deutscher Chemiker

Angewandte International Edition Chemie

GDCh

www.angewandte.org

Accepted Article

Title: Visualization of Colorectal Cancers Using Activatable Nanoprobes with Second Near-Infrared Emissions

Authors: Ge Xu, Qinglong Yan, Xiaoguang Lv, Ying Zhu, Kai Xin, Ben Shi, Rongchen Wang, Jian Chen, Wei Gao, Ping Shi, Chunhai Fan, Chunchang Zhao, and He Tian

To be cited as: *Angew. Chem. Int. Ed.* 10.1002/anie.201712528
Angew. Chem. 10.1002/ange.201712528

Link to VoR: http://dx.doi.org/10.1002/anie.201712528
http://dx.doi.org/10.1002/ange.201712528

WILEY-VCH

10.1002/anie.201712528

WILEY-VCH

Visualization of Colorectal Cancers Using Activatable Nanoprobes with Second Near-Infrared Emissions

Ge Xu,[a,†] Qinglong Yan,[b,†] Xiaoguang Lv,[c] Ying Zhu,*,[b] Kai Xin,[a] Ben Shi,[a] Rongchen Wang,[a] Jian Chen,[a] Wei Gao,[a] Ping Shi,[c] Chunhai Fan,*,[b] Chunchang Zhao,*,[a] He Tian[a]

Abstract: Fluorescent probes in the second near-infrared window (NIR-II) allow high-resolution bioimaging with deep-tissue penetration. However, existing NIR-II materials often have poor signal-to-background ratios due to the lack of target specificity. Herein, we devised an activatable NIR-II nanoprobe for visualizing colorectal cancers. This designed probe possessed H_2S-activated ratiometric fluorescence and light-up NIR-II emission of 900-1300 nm. By using this activatable and target specific probe for deep-tissue imaging of H_2S-rich colon cancer cells, we realized accurate identification of colorectal tumors in animal models. We thus anticipate that the development of activatable NIR-II probes will find widespread applications in biological and clinical systems with high precision and resolution.

Optical imaging is an essential tool for biological research and biomedical applications due to the advantages of lower cost, simple operation, noninvasive and real time capabilities.[1] Specially, fluorescence imaging provides a powerful approach for early detection and management of malignant tumors. For example, fluorescent probes with emission at visible region can selectively monitor intra- and extracellular cancer biomarkers by readily coupling with the widely available biological imaging instruments such as confocal and epifluorescence light microscopy.[2] Although these great advances, conventional fluorescence imaging still suffers from a lot of concerns regarding the limited tissue penetration, poor spatial resolution inside deep biological tissue and disturbance by strong autofluorescence from living tissues, which have largely restricted their applications in living animals.[3]

Recent progresses have demonstrated that fluorescent imaging in the second near-infrared window (NIR-II, 1000–1700 nm) can provide solutions for addressing the abovementioned multiple issues, showing reduced autofluorescence, lower tissue absorption, greatly improved tissue penetration depth and higher in vivo spatial resolution compared to visible (450–750 nm) and traditional NIR-I imaging (750–900 nm).[4] Indeed, several materials have been applied as NIR-II fluorophores non-invasively to visualize biological events in a living subject, including small-molecule dyes, metallic nanoparticles, carbon nanotubes, quantum dots and rare earth nanoparticles.[5-9] However, the NIR-II fluorescence signals are often not directly associated with interactions of imaging agents with the targets of interest, resulting in poor signal-to-background ratios. Thus accurately measuring anatomical features or biological events of interest with NIR-II probes remains challenging. As an alternative strategy, activatable probes that undergo intrinsic signal evolution only in response to specific biological targets or events can amplify signals from the target and suppress background.[10] However, few activatable materials with NIR-II emissions have been explored for biological imaging applications. Herein, we reported an activatable probe with emission in the NIR-II region for visualizing colorectal cancers by full utilization of the merits of NIR-II imaging at a depth and spatial resolution.

In this contribution, we demonstrated our design concept by fabrication of nanoprobes through encapsulating a H_2S-responsive fluorescent probe into the hydrophobic interior of core–shell silica nanocomposites, considering that the overexpressed H_2S-producing enzyme cystathionine-β-synthase (CBS) in colon cancer gives rise to increased H_2S production.[11] In fact, increased H_2S production is closely linked to various cancers, including ovarian, breast and colorectal cancers.[11b] Thereby, H_2S can be regard as a biomarker for cancer diagnosis as well as a therapeutic potential on these tumors. Undoubtedly, H_2S-activated emissions in NIR-II window could provide valuable insight into accurate location of colorectal cancers.

The activatable nanoprobes are comprised of two organic chromophores: a rational designed boron-dipyrromethene (ZX-NIR) dye to generate the NIR-II emission only in the presence of H_2S, and an aza-BODIPY (aza-BOD) that is inert to H_2S, serving as the internal reference. Such a design is to construct probes with multi-emission for ratiometric imaging, as multi-wavelength imaging is promising in acquiring high precision measurements.[12] As shown in Figure 1, the designed nanoprobes were fabricated in two steps: 1) trapping the two dyes ZX-NIR and aza-BOD into the hydrophobic interior of self-assembled micellar aggregate based on 1,2-dimyristoyl-*sn*-glycero-3-phosphoethanolamine-N-[methoxy(polyethylene glycol)-2000] (mPEG-DSPE); 2) in situ shell cross-linking with (N-trimethoxysilylpropyl-N,N,N-tri-n-butylammonium bromide (TBNBr)) to produce water-dispersible core-shell silica nanocomposites (NIR-II@Si) with a covalently cross-linked silica shell. As a result, the silica cross-linkers realize the buildup a shield for stable confinement of the two dyes within the same cavity of these nanoparticles.[13] Furthermore, such silica nanoparticles has the advantage of good water-solubility and excellent biocompatibility as well as fast responsiveness.

We have employed the dye-screening approach for affording probes with good responsiveness (Figure 1 and Scheme S1).

[a] G. Xu, K. Xin, B. Shi, R. Wang, J. Chen, W. Gao, Prof. C. Zhao, Prof. H. Tian
Key Laboratory for Advanced Materials and Institute of Fine Chemicals, School of Chemistry and Molecular Engineering
East China University of Science and Technology
Shanghai 200237, P. R. China
E-mail: zhaocchang@ecust.edu.cn
[b] Q. Yan, Prof. Y. Zhu, Prof. C. Fan
Division of Physical Biology & Bioimaging Center, Shanghai Institute of Applied Physics
Chinese Academy of Sciences
Shanghai 201800, P. R. China
E-mail: zhuying@sinap.ac.cn, fchh@sinap.ac.cn
[c] X. Lv, Prof. P. Shi
State Key Laboratory of Bioreactor Engineering
East China University of Science and Technology
Shanghai 200237, P. R. China
† These authors contributed equally.

Supporting information for this article is given via a link at the end of the document.

The reactivity toward H_2S was evaluated by fluorescence analysis. As shown in Figure S1, compound **1** gave no fluorescence response to H_2S in CH_3CN/PBS buffer mixtures (1:1, v/v, 20 mM, pH 7.4, room temperature). As seen for compound **3**, enhancement of the electron deficiency of BODIPY core by appending electron-withdrawing units increased the reactivity toward H_2S. Based on these preliminary studies, we finally attached a better leaving group 4-nitrobenzenethiol instead of p-thiocresol for affording the optimized model probe ZX-NIR.

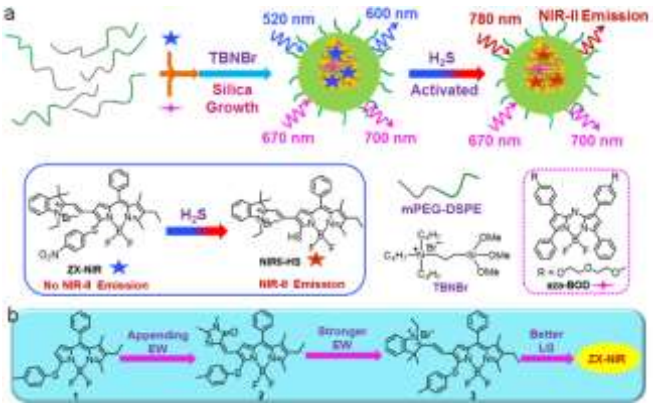

Figure 1. (a) Schematic illustration of the construction of multi-wavelength nanoprobes with activatable emissions in the second near-infrared window. (b) The dye-screening approach for rational design of probes for H_2S. EW: electron withdrawing; LG: leaving group.

In the absence of H_2S, ZX-NIR shows intense absorption at 520 nm and emission band at 600 nm in CH_3CN/PBS buffer mixtures (1:1, v/v, 20 mM, pH 7.4, room temperature). When exposed to 100 μM NaHS (a commonly employed H_2S donor), a new absorption band around 740 nm was built up and the original absorption at 520 nm was reduced concomitantly (Figure S2), showing a remarkable red-shift of 220 nm. Upon excitation at 520 nm, the fluorescence at 600 nm showed a time-dependent quenching. Fortunately, a new NIR-II emission, with maximum emission peak of 900 nm, was activated in the presence of H_2S when the excitation wavelength was 740 nm. Generally, the spectral range of fluorophores in NIR-II window is considered to be between 1000 and 1700 nm. Although H_2S-triggered maximum emission wavelength lies at 900 nm, the emission spectrum is quite broad and extends into the region (1000-1300 nm) of NIR-II. These changes were ascribed to the transformation of ZX-NIR into NIRII-HS through aromatic nucleophilic substitution (S_NAr), confirmed by HRMS analysis (Figure S3).

According to reaction-time study, the reaction of 240 min between ZX-NIR and H_2S was found to be comparable with that of most reported H_2S probes (30−200 min).[14] However, such reaction rate is not fast enough to image the transient H_2S. To address the issue of the limited solubility of ZX-NIR as well as its relatively slow reaction with H_2S in aqueous solution, ZX-NIR and aza-BOD at the molar ratio of 3:1 were then incorporated into the hydrophobic interior of water-dispersible NIR-II@Si following our established method.[13] Aza-BODIPY was selected as it has high absorption and emission at 670 nm and 700 nm, respectively, which are well-resolved and mutually poor-overlapping with those of ZX-NIR and the activated form NIRII-HS, thus acting as an internal inference. The resulting water dispersible nanocomposites were fully characterized by dynamic light scattering (DLS) and transmission electron microscopy (TEM) (Figure S4). NIR-II@Si was found to be stable in aqueous solution. The particle diameters remained at 66 nm and no aggregation was found in the suspension for days (Figure S4). The loading contents of ZX-NIR and aza-BODIPY in NIR-II@Si nanocomposites were determined to be 0.39 and 0.10 wt %, respectively, according to the standard UV–vis–NIR absorbance spectra.

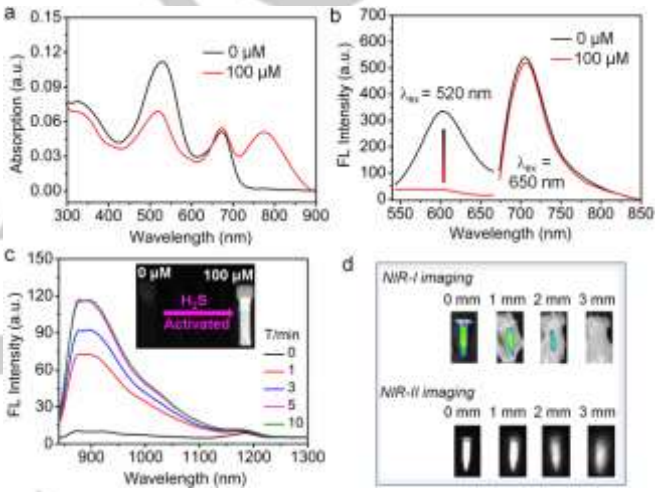

Figure 2. (a) Absorption and (b) fluorescence changes of NIR-II@Si (10 μM ZX-NIR) upon addition with 100 μM NaHS in PBS buffer solution (pH 7.4). (c) Time dependent NIR-II emission spectra of NIR-II@Si (10 μM ZX-NIR) in the presence of 100 μM NaHS, λ_{ex} = 780 nm. Inset is the photograph of the H_2S-activated NIR-II emission. (d) The comparison of NIR-I and NIR-II fluorescence imaging of samples covered by pork tissues.

The optical response of NIR-II@Si toward H_2S was studied in PBS buffer solutions (pH 7.4). It was found that ZX-NIR showed dramatic optical response to H_2S within the water-dispersible nanocomposites. Upon reaction with NaHS (100 μM), the NIR absorption at 780 nm was generated, accompanied by the reduction of the peak at 520 nm (Figure 2). Such treatment with NaHS induced the completely quenching the emission at 600 nm (excitation at 520 nm) within 5 min (Figure S5). Specifically, a robust increase in fluorescence intensity within NIR-II window was observed when the excitation wavelength was 780 nm, reaching a plateau within 5 min which allows for monitoring of H_2S-related biological processes in real-time. This process triggered a bright NIR-II image with the relative quantum yield of 0.37% under 810-nm laser irradiation (Figure 2c inset). In contrast, the absorbance and fluorescence of aza-BOD, different from that of ZX-NIR, are inert to H_2S. Therefore, the absorbance peak at 670 nm and fluorescence at 700 nm showed no appreciable change in the presence of NaHS. Interestingly, the fluorescence intensity ratio of I_{700}/I_{600} increased

with the gradual increase of NaHS concentrations, affording a good linear relationship within the concentration range from 0 to 10 μM. The detection limit was measured to be 37 nM, indicating the high sensitivity of NIR-II@Si for ratiometric detection of H_2S. The capability of NIR-II@Si to produce both NIR-I fluorescence (emission of aza-BOD at 700 nm) and activatable NIR-II signals (emission of NIRII-HS at 900 nm) enabled a direct comparison of NIR-I and NIR-II fluorescence imaging in terms of NIR-II@Si performance. The polyethylene tube was covered by pork tissues with different thicknesses and subjected to imaging. As shown in Figure 2d and Figure S5, the NIR-II fluorescence signal of NIR-II@Si was detectable even through a 10 mm pork tissue. In sharp contrast, the NIR-I fluorescence was attenuated to the background level for samples covered by just a 3 mm pork tissue. These results clearly demonstrate that NIR-II imaging is a preferred technique over NIR-I fluorescence imaging for providing better spatial resolution and deeper penetration depths. Combined, advantages including ratiometric fluorescence and light-up NIR-II emission enable NIR-II@Si a promising tool for preclinical applications in both living cells and animals with high precision and resolution.

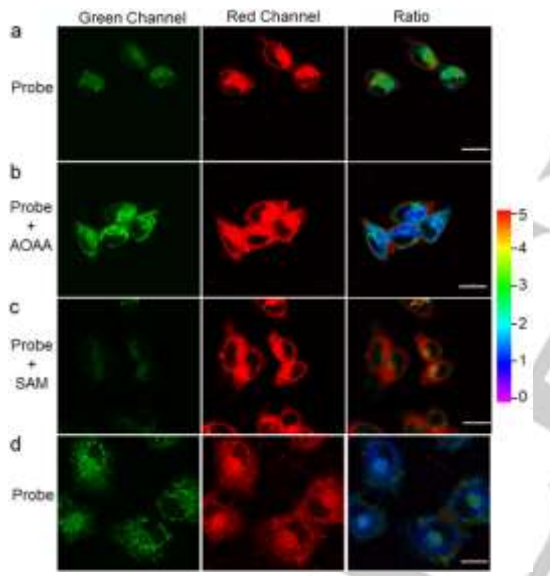

Figure 3. Identification of colon cancer cells by confocal microscopy images in dual-color imaging modality. (a) HCT116 cells incubated with NIR-II@Si (ZX-NIR 10 μM) for 30 min. (b) HCT116 cells pretreated with 1 mM AOAA for 1h, followed by incubation with NIR-II@Si for 30 min. (c) HCT116 cells pretreated with SAM (3mM) for 1 h were loaded with NIR-II@Si for 30 min. (d) HepG2 cells incubated with NIR-II@Si for 30 min. The excitation wavelength was 561 nm, green channel at 600−630 nm, red channel at 700−750 nm; ratio images generated from red channel to green channel. Scale bar: 20 μM.

NIR-II@Si exhibited high selectivity for H_2S compared to a panel of biologically related analytes, including reactive sulfur (RSS), oxygen (ROS), and nitrogen species (RNS). As shown in Figure S6, these inferring species caused negligible fluctuation of fluorescence within 900-1300 nm, whereas the introduction of NaHS triggered a prominent enhancement of the NIR-II fluorescence intensity. The ratiometric fluorescence mode (I_{700}/I_{600}) also gave an accurate estimation of the selectivity. Only NaHS induced a significant enhancement in the fluorescence intensity ratio (I_{700}/I_{600}), while other analytes gave no obvious ratiometric changes. In addition, experiments for the pH effect on the response to H_2S revealed that NIR-II@Si afforded good optical response within a physiological range from pH 9 to approximately 5 (Figure S7). Notably, the core-shell structured NIR-II@Si showed good photostability in aqueous solution (Figure S8). Minimal fluorescence spectra change was observed after being stored for 24 h or under continuous irradiation for 2 h with an Hg/Xe lamp.

Since overexpressed CBS promotes high levels of H_2S in human colon cancers, the ability to selective identification of colon cancer cells was studied by tracking of increased H_2S production in dual-color imaging modality. Human hepatocellular liver carcinoma cells (HepG2 cells) were used as a control due to the minimized level of H_2S in these cells. After validating low cytotoxicity of NIR-II@Si (Figure S9), human colorectal cancer HCT116 cells were then loaded with NIR-II@Si for 30 minutes. Bright and stable fluorescence signals were noted in the red channel, while relatively weak fluorescence signals were observed in the green channel (Figure 3). The ratio of the red channel to green channel was used for quantification of images. HCT116 cells incubated with NIR-II@Si showed a ratio of approximately 3.0 (Figure S9). Such ratio of the red-to-green signal was significantly attenuated by the addition of a CBS inhibitor aminooxyacetic acid (AOAA) due to the inhibition effect on the cellular H_2S production. In contrast, stimulation of cells with an allosteric CBS activator S-adenosyl-L-methionine (SAM) resulted in dramatic elevation of red-to-green image ratio to 4.5. These imaging results demonstrated the feasibility of NIR-II@Si to specially image colon cancer cells by monitoring of the elevated production of H_2S. To further validate the obtained assumption, control experiments with HepG2 cells were performed. As shown in Figure S9, HepG2 cells showed strong fluorescence in both green and red channels with the red-to-green signal ratio of 1.4. Different from that in HCT116 cells, almost no change of fluorescence ratio was observed when HepG2 cells were pretreated with AOAA or SAM. All the results indicate that NIR-II@Si can be used to differentiate types of living cells, based on their difference in H_2S contents.

NIR-II@Si was further explored for visualization of colorectal cancers in vivo by full utilization of its promising light-up NIR-II emission in response to H_2S. In this study, HCT116 subcutaneous xenograft nude mice were established due to high levels of H_2S in HCT116 cells. HCT116 tumor-bearing mice were administrated by intratumoral injection of NIR-II@Si. NIR-II@Si was also injected into the normal muscle of a mouse to confirm the advantage of activatable probes over “always-on” probes. Then images were recorded at various times after the injection (Figure 4 and Figure S10). Strong NIR-II emission was noted specifically in the tumor region within 1 min post-injection of the probe, while barely detectable fluorescence was observed in the normal site injected with the probe. Such specific NIR-II signals in the tumors increased with time and eventually leveled off in 30 min after probe injection. According to region of interest measurements, the NIR-II signal ratio between the tumor and normal site (T/N) was estimated to be 5.7 (20 min) (Figure S10). Considering the “always-on” NIR-I fluorescence of NIR@Si from aza-BOD, the NIR-I fluorescent signals were observed in both

the tumor site and normal muscle immediately after the injection. Minimal fluorescence changes of the two sites could be noted within 30 min and the T/N ratio is approximately 1.0. Hence, "always-on" probes subject to the lack of target specificity and thus have no opportunity for signal amplification, which could reduce the sensitivity of the probe. By contrast, the activatable NIR-II signals afford higher tumor–to–normal tissue ratios than "always-on" probes. Furthermore, the advantage of NIR-II imaging over NIR-I imaging was also demonstrated using NIR-II@Si in a simulated deep-tissue setting (Figure S11). Bright NIR-II signal from NIR-II@Si could be clearly visualized even at a depth of 10 mm while the NIR-I fluorescence signal was invisible above 2 mm. To further validate that the NIR-II signals was indeed activated by H_2S in colorectal cancers, pretreatment of tumor sites with a CBS inhibitor AOAA or an allosteric CBS activator SAM were performed. Experimental results showed that AOAA effectively suppressed the NIR-II fluorescence signals in the tumor while SAM greatly facilitated the elevation of NIR-II signals. These results suggested that NIR-II@Si provides a reliable tool for visualization of colorectal cancers by trapping transient H_2S. To explore the possibility of differentiating types of cancers based on H_2S content, the HepG2 tumor-bearing mouse model was then subjected to in vivo imaging due to low level of H_2S in HepG2 cells. As expected, minimal NIR-II emission was activated in HepG2 tumors. In sharp contrast, clear NIR-I signals was observed in these sites due to the "always on" feature of aza-BOD in NIR-II@Si (Figure 4d). These results clearly demonstrated that the NIR-II fluorescence of NIR-II@Si preferentially light up in H_2S-rich cancers, rather than in H_2S-deficient cancers and non-cancerous tissues. Taken together, cancers can be rapidly visualized and differentiated based on H_2S activation of NIR-II@Si.

Next, in vivo biodistribution and pharmacokinetics studies were conducted by intravenous injection of NIR-II@Si into HCT116 tumor-bearing mice. The NIR-II fluorescence could hardly be observed within 24 h post the tail veil injection, suggesting limited passive tumor uptake of NIR-II@Si in the absence of a targeting ligand.[15] To evaluate the biodistribution of NIR-II@Si, we recorded the ex vivo fluorescence imaging of tumor and various organs (liver, lung, spleen, heart, and kidney). The high uptake of NIR-II@Si was observed in kidney and liver, while tumor and other major organs showed low uptake (Figure S12). Furthermore, pharmacokinetics study indicated that NIR-II@Si exhibited only 3% retentions in blood stream at 60 min post intravenous injection (Figure S13). In addition, blood analysis including hematology and blood biochemical indicators suggested low in vivo toxicity of NIR-II@Si (Table S1).

In summary, we have fabricated an activatable nanoprobe with emission in the NIR-II window for visualizing colorectal cancers. This nanoprobe showed specific and ratiometric fluorescence responsiveness to H_2S, thus enabling the selective identification of H_2S-rich colon cancer cells and differentiation between types of living cells based on their difference in H_2S contents in a dual-color imaging modality. More importantly, H_2S specifically activated the fluorescence in NIR-II region which allowed in vivo detection and differentiation of cancers by full utilization of the merits of NIR-II imaging at a depth and spatial resolution. We expect that our design approach could facilitate the development of smart activatable probes to advance the NIR-II imaging in biology and medicine.

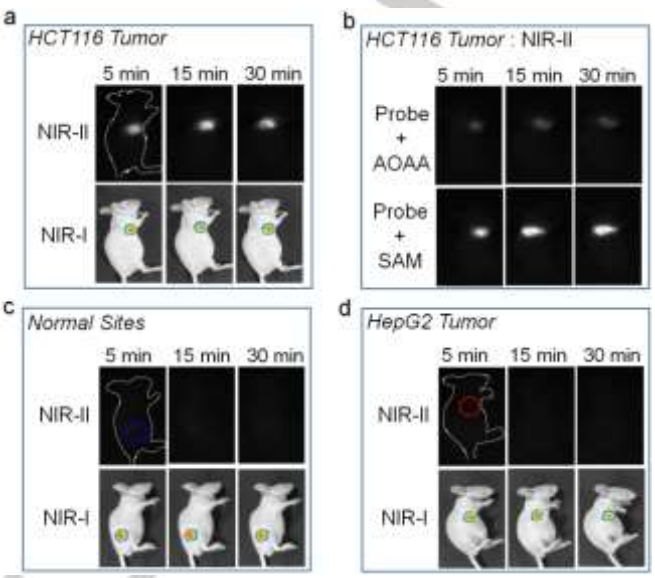

Figure 4. Visualization and differentiation of cancers based on H_2S activation of NIR-II@Si (20 nmol ZX-NIR). The tumor regions and normal muscle of living mice were subcutaneously treated with the probe, and images were taken at various time points after injection. (a) HCT116 tumor bearing mice. (b) The effects of inhibitor (AOAA) and activator (SAM) in HCT116 tumor bearing mice. (c) Normal sites. (d) HepG2 tumor bearing mice.

Acknowledgements

We gratefully acknowledge the financial support by the National Science Foundation of China (grant numbers 21672062, 21421004, 11675251, 21390414), the Programme of Introducing Talents of Discipline to Universities (B16017), National Key R&D Program of China (2016YFA0201200, 2016YFA0400900), and the Key Research Program of Frontier Sciences, CAS (Grant NO.QYZDJ-SSW-SLH031).

Keywords: second near-infrared • activatable • nanoprobe • colon cancer • in vivo

[1] a) R. Weissleder, M. J. Pittet, *Nature* **2008**, *452*, 580; b) Y. Yang, Q. Zhao, W. Feng, F. Li, *Chem. Rev.* **2013**, *113*, 192; c) J. Liang, B. Z. Tang, B. Liu, *Chem. Soc. Rev.* **2015**, *44*, 2798; d) M. H. Lee, J. S. Kim and J. L. Sessler, *Chem. Soc. Rev.* **2015**, *44*, 4185.

[2] a) F. Wang, Y. Zhu, L. Zhou, L. Pan, Z. Cui, Q. Fei, S. Luo, D. Pan, Q. Huang, R. Wang, C. Zhao, H. Tian, C. Fan, *Angew. Chem. Int. Ed.* **2015**, *54*, 7349-; b) L. Yuan, W. Lin, S. Zhao, W. Gao, B. Chen, L. He, S. Zhu, *J. Am. Chem. Soc.* **2012**, 134, 13510; c) H. Zhu, J. Fan, J. Du, X. Peng, *Acc. Chem. Res.* **2016**, *49*, 2115; d) S. Wang, S. Deng, X. Cai, S. Hou, J. Li, Z. Gao, J. Li, L. Wang, C. Fan, *Sci. China Chem.* **2016,** *59,* 1519; e) M. Schäferling, *Angew. Chem. Int. Ed.* **2012**, *51*, 3532; e) K. Li, B. Liu, *Chem. Soc. Rev.* **2014**, *43*, 6570.

[3] a) L. Xiong, A. J. Shuhendler, J. Rao, *Nat. Commun.* **2012**, *3*, 1193; b) L. Zhou, X. Zhang, Q. Wang, Y. Lv, G. Mao, A. Luo, Y. Wu, Y. Wu, J. Zhang, W. Tan, *J. Am. Chem. Soc.* **2014**, 136, 9838.

[4] a) G. Hong, J. C. Lee, J. T. Robinson, U. Raaz, L. Xie, N. F. Huang, J. P. Cooke, H. Dai, *Nat. Med.* **2012**, *18*, 1841; b) D. Naczynski, M. Tan, M. Zevon, B. Wall, J. Kohl, A. Kulesa, S. Chen, C. Roth, R. Riman, P. Moghe, *Nat. Commun.* **2013**, *4*, 2199; c) X. Dang, L. Gu, J. Qi, S. Correa, G. Zhang, A. M. Belcher, P. T. Hammond, *Proc. Natl. Acad. Sci. USA* **2016**, *113*, 5179; d) G. Hong, Y. Zou, A. L. Antaris, S. Diao, D. Wu, K. Cheng, X. Zhang, C. Chen, B. Liu, Y. He, J. Z. Wu, J. Yuan, B. Zhang, Z. Tao, C. Fukunaga, H. Dai, *Nat. Commun.* **2014**, *5*, 4206.

[5] a) Q. Yang, Z. Ma, H. Wang, B. Zhou, S. Zhu, Y. Zhong, J. Wang, H. Wan, A. Antaris, R. Ma, X. Zhang, J. Yang, X. Zhang, H. Sun, W. Liu, Y. Liang, H. Dai, *Adv. Mater.* **2017**, *29*, 1605497; b) A. L. Antaris, H. Chen, K. Cheng, Y. Sun, G. Hong, C. Qu, S. Diao, Z. Deng, X. Hu, B. Zhang, X. Zhang, O. K. Yaghi, Z. R. Alamparambil, X. Hong, Z. Cheng, H. Dai, *Nat. Mater.* **2016**, *15*, 235; c) X.-D. Zhang, H. Wang, A. L. Antaris, L. Li, S. Diao, R. Ma, A. Nguyen, G. Hong, Z. Ma, J. Wang, S. Zhu, J. M. Castellano, T. Wyss-Coray, Y. Liang, J. Luo, H. Dai, *Adv. Mater.* **2016**, *28*, 6872; d) K. Shou, C. Qu, Y. Sun, H. Chen, S. Chen, L. Zhang, H. Xu, X. Hong, A. Yu, Z. Cheng, *Adv. Funct. Mater.* **2017**, *27*, 1700995; e) E. D. Cosco, J. R. Caram, O. T. Bruns, D. Franke, R. A. Day, E. P. Farr, M. G. Bawendi, E. M. Sletten, *Angew. Chem. Int. Ed.* **2017**, *56*, 13126; f) A. L. Antaris, H. Chen, S. Diao, Z. Ma, Z. Zhang, S. Zhu, J. Wang, A. X. Lozano, Q. Fan, L. Chew, M. Zhu, K. Cheng, X. Hong, H. Dai, Z. Cheng, *Nat. Commun.* **2017**, *8*, 15269; g) S. Zhu, Q. Yang, A. L. Antaris, J. Yue, Z. Ma, H. Wang, W. Huang, H. Wan, J. Wang, S. Diao, B. Zhang, X. Li, Y. Zhong, K. Yu, G. Hong, J. Luo, Y. Liang, H. Dai, *Proc. Natl. Acad. Sci. U. S. A.* **2017**, *114*, 962; h) Z. Tao, G.Hong, C. Shinji, C. Chen, S. Diao, A. L. Antaris, B. Zhang, Y. Zou, H. Dai, *Angew. Chem. Int. Ed.* **2013**, *52*, 13002; i) Y. Sun, C. Qu, H. Chen, M. He, C. Tang, K. Shou, S. Hong, M. Yang, Y. Jiang, B. Ding, Y. Xiao, L. Xing, X. Hong, Z. Cheng, *Chem. Sci.* **2016**, *7*, 6203.

[6] L. Fang, Y. Wang, M. Liu, M. Gong, A. Xu, Z. Deng, *Angew. Chem. Int. Ed.* **2016**, *55*, 14296.

[7] a) K. Welsher, Z. Liu, S. P. Sherlock, J. T. Robinson, Z. Chen, D. Daranciang, H. Dai, *Nat. Nanotechnol.* **2009**, *4*, 773; b) G. Hong, J. Z. Wu, J. T. Robinson, H. Wang, B. Zhang, H. Dai, *Nat. Commun.* **2012**, *3*, 700; c) G. Hong, S. Diao, J. Chang, A. L. Antaris, C. Chen, B. Zhang, S. Zhao, D. N. Atochin, P. L. Huang, Andreasson, K. I. C. J. Kuo, H. Dai, *Nat. Photonics* **2014**, *8*, 723; d) N. M. Iverson, P. W. Barone, M. Shandell, L. J. Trudel, S. Sen, F. Sen, V. Ivanov, E. Atolia, E. Farias, T. P. McNicholas, N. Reuel, N. M. A. Parry, G. N. Wogan, M. S. Strano, *Nat. Nanotechnol.* **2013**, *8*, 873.

[8] a) G. Hong, J. T. Robinson, Y. Zhang, S. Diao, A. L. Antaris, Q. Wang, H. Dai, *Angew. Chem. Int. Ed.* **2012**, *51*, 9818; b) G. Chen, F. Tian, C. Li, Y. Zhang, Z. Weng, Y. Zhang, R. Peng, Q. Wang, *Biomaterials*, **2015**, *53*, 265; c) S. Jeong, J. Song, W. Lee, Y. M. Ryu, Y. Jung, S.-Y. Kim, K. Kim, S. C. Hong, S. J. Myung, S. Kim, *Nano Lett.* **2017**, *17*, 1378.

[9] W. Shao, G. Chen, A. Kuzmin, H. L. Kutscher, A. Pliss, T. Y. Ohulchanskyy, P. N. Prasad, *J. Am. Chem. Soc.* **2016**, *138*, 16192.

[10] a) L. Yuan, W. Lin, K. Zheng, L. He, W. Huang, *Chem. Soc. Rev.* **2013**, *42*, 622; b) Z. Zhao, H. Fan, G. Zhou, H. Bai, H. Liang, R. Wang, X. Zhang, W. Tan, *J. Am. Chem. Soc.* **2014**, *136*, 11220; c) A. Razgulin, N. Ma, J. H. Rao, *Chem. Soc. Rev.* **2011**, *40*, 4186–4216; d) M. Whitney, E. N. Savariar, B. Friedman, R. A. Levin, J. L. Crisp, H. L. Glasgow, R. Lefkowitz, S. R. Adams, P. Steinbach, N. Nashi, Q. T. Nguyen, R. Y. Tsien, *Angew. Chem. Int. Ed.* **2013**, *52*, 325; e) E. S. Olson, T. Jiang, T. A. Aguilera, Q. T. Nguyen, L. G. Ellies, M. Scadeng, R. Y. Tsien, *Proc. Natl. Acad. Sci.* **2010**, *107*, 4311.

[11] a) C. Szabo, C. Coletta, C. Chao, K. M´odis, B. Szczesny, A. Papapetropoulos and M. R. Hellmich, *Proc. Natl. Acad. Sci. U. S. A.* **2013**, *110*, 12474; b) C. Szabo, *Nat. Rev. Drug Discovery* **2016**, *15*, 185; c) B. Shi, X. Gu, Q. Fei, C. Zhao, *Chem. Sci.* **2017**, *8*, 2150; d) Y. Ma, X. Li, A. Li, P. Yang, C. Zhang, B. Tang, *Angew. Chem. Int. Ed.* **2017**, *56*, 13752.

[12] a) L.-Y. Niu, Y.-Z. Chen, H.-R. Zheng, L.-Z. Wu, C.-H. Tung, Q.-Z. Yang, *Chem. Soc. Rev.* **2015**, *44*, 6143; b) H. S. Jung, X. Chen, J. S. Kim, J. Yoon, *Chem. Soc. Rev.* **2013**, *42*, 6019.

[13] B. Shi, X. Gu, Z. Wang, G. Xu, Q. Fei, J. Tang, C. Zhao, *ACS Appl. Mater. Interfaces* **2017**, *9*, 35588.

[14] a) V. S. Lin, W. Chen, M. Xian, C. J. Chang, *Chem. Soc. Rev.* **2015**, *44*, 4596; b) X. Zhou, S. Lee, Z. Xu, J. Yoon, *Chem. Rev.* **2015**, *115*, 7944; c) M. D. Hammers, M. J. Taormina, M. M. Cerda, L. A. Montoya, D. T. Seidenkranz, R. Parthasarathy, M. D. Pluth, *J. Am. Chem. Soc.* **2015**, *137*, 10216; d) L. Zhang, H. Zhu, M. Li, X. Gu, *Chem. Commun.* **2015**, *51*, 13135; e) W. Zhang, J. Kang, P. Li, H. Wang, B. Tang, *Anal. Chem.* **2015**, *87*, 8964; f) C. Zhao, X. Zhang, K. Li, S. Zhu, Z. Guo, L. Zhang, F. Wang, Q. Fei, S. Luo, P. Shi, H. Tian, W.-H. Zhu, *J. Am. Chem. Soc.* **2015**, *137*, 8490; g) K. Zhang, J. Zhang, Z. Xi, L.-Y. Li, X. Gu, Q.-Z. Zhang, L. Yi, *Chem. Sci.* **2017**, *8*, 2776.

[15] Z. Liu, W. Cai, L. He, N. Nakayama, K. Chen, X. Sun, X. Chen, H. Dai, *Nat. Nanotech.* **2007**, *2*, 47.

10.1002/anie.201712528

WILEY-VCH

Entry for the Table of Contents

COMMUNICATION

NIR-II emission: Activatable Nanoprobes with second near-infrared emissions were constructed. Such designed probes possessed H_2S-activated ratiometric fluorescence and light-up NIR-II emission, realizing the specific imaging of H_2S-rich colon tumour and differentiation of types of cancers.

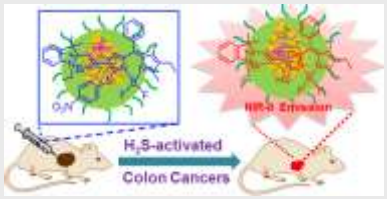

Ge Xu, Qinglong Yan, Xiaoguang Lv, Ying Zhu, Kai Xin, Ben Shi, Rongchen Wang, Jian Chen, Wei Gao, Ping Shi, Chunhai Fan,* Chunchang Zhao,* He Tian*

Page No. – Page No.

Visualization of Colorectal Cancers Using Activatable Nanoprobes with Second Near-Infrared Emissions